



ELSEVIER

NeuroImage

www.elsevier.com/locate/ynimg
NeuroImage xx (2007) xxx–xxx

Topography of cortical and subcortical connections of the human pedunclopontine and subthalamic nuclei

B.R. Aravamuthan,^{a,b,*} K.A. Muthusamy,^a J.F. Stein,^a T.Z. Aziz,^c and H. Johansen-Berg^d

^aDepartment of Physiology, Anatomy, and Genetics, Sherrington Building, University of Oxford, Parks Road, Oxford, OX1 3PT, UK

^bNational Institute of Neurological Disorders and Stroke, Bethesda, MD, USA

^cDepartment of Neurological Surgery, Radcliffe Infirmary, Oxford, UK

^dOxford Centre for Functional MRI of the Brain, John Radcliffe Hospital, Oxford, UK

Received 6 February 2007; revised 14 April 2007; accepted 18 May 2007

Deep brain stimulation (DBS) of the subthalamic nucleus (STN) is the most common surgical therapy for Parkinson's disease (PD). DBS of the pedunclopontine nucleus (PPN) is emerging as a promising surgical therapy for PD as well. In order to better characterize these nuclei in humans, we determined the anatomical connections of the PPN and STN and the topography of these connections using probabilistic diffusion tractography. Diffusion tractography was carried out in eight healthy adult subjects using diffusion data acquired at 1.5 T MRI (60 directions, $b=1000$ s/mm², $2 \times 2 \times 2$ mm³ voxels). The major connections that we identified from single seed voxels within STN or PPN were present in at least half the subjects and the topography of these connections within a 36-voxel region surrounding the initial seed voxel was then examined. Both the PPN and STN showed connections with the cortex, basal ganglia, cerebellum, and down the spinal cord, largely matching connections demonstrated in primates. The topography of motor and associative brain areas in the human STN was strikingly similar to that shown in animals. PPN Topography has not been extensively demonstrated in animals, but we showed significant topography of cortical and subcortical connections in the human PPN. In addition to demonstrating the usefulness of PDT in determining the connections and topography of small grey matter structures *in vivo*, these results allow for inference of optimal DBS target locations and add to our understanding of the role of these nuclei in PD.

© 2007 Elsevier Inc. All rights reserved.

Introduction

Deep brain stimulation (DBS) of specific nuclei can alleviate intractable Parkinson's disease (PD) symptoms. The subthalamic nucleus (STN) is currently the most common target and stimulation of this structure is particularly successful in reducing tremor and

bradykinesia (Limousin et al., 1995; Krack et al., 1997; Limousin et al., 1998; Yokoyama et al., 1999; Bejjani et al., 2000; Stolze et al., 2001; Kleiner-Fisman et al., 2003; Rodriguez-Oroz et al., 2005). Recent evidence suggests that stimulation of the pedunclopontine nucleus (PPN) in the upper brainstem can be effective in ameliorating medically intractable akinesia (Jenkinson et al., 2004; Plaha and Gill, 2005; Mazzone et al., 2005; Galati et al., 2006). In both cases, the effects of stimulation are not limited to the targeted structure but will affect the distributed anatomical networks to which the target structure belongs. Therefore, understanding the anatomical connections of these deep brain structures will help elucidate treatment effects. In particular, establishing the topography of cortical and subcortical connections of STN and PPN in the human brain could help with accurate targeting of critical pathways in DBS.

The PPN plays an important role in controlling movement, particularly of the axial and proximal limb muscles employed in the maintenance of posture and locomotion (Masdeu et al., 1994; Lee et al., 2000; Pahapill and Lozano, 2000). While lesions to the PPN cause akinesia (Kojima et al., 1997; Munro-Davies et al., 1999; Matsumura and Kojima, 2001), stimulation (Jenkinson et al., 2004) or disinhibition (Nandi et al., 2002) of the PPN can dramatically improve motor behavior in monkeys made parkinsonian with MPTP, suggesting that the PPN is over inhibited by the basal ganglia in Parkinson's disease. Hence, deep brain stimulation of the PPN has been tested in Parkinsonian patients and early results show promising outcomes particularly in reducing akinesia and gait abnormalities (Plaha and Gill, 2005; Mazzone et al., 2005).

The need for accurate surgical targeting of the PPN for DBS procedures necessitates better anatomical characterization of the PPN. Currently, PPN connections have been best characterized using tracing and evoked-potential studies in rodents (Garcia-Rill et al., 1987; Rye et al., 1987; Garcia-Rill and Skinner, 1987a; Garcia-Rill and Skinner, 1987b; Spann and Grofova, 1989; Spann and Grofova, 1991; Spann and Grofova, 1992), but these connections differ greatly from those shown in primate tracing studies (Lavoie and Parent, 1994a,b,c; Pahapill and Lozano, 2000). Though both the rodent and primate PPN have strong connections with the

* Corresponding author. Department of Physiology, Anatomy, and Genetics, Sherrington Building, University of Oxford, Parks Road, Oxford, OX1 3PT, UK. Fax: +44 1865272469.

E-mail address: bhooma.aravamuthan@dpag.ox.ac.uk.

Available online on ScienceDirect (www.sciencedirect.com).

78 subthalamic nucleus (STN), substantia nigra (SN), and globus
79 pallidus (GP) (Lee et al., 2000), connections between the PPN and
80 motor cortex have only been shown in primates, and projections
81 from the PPN to the deep cerebellar nuclei and projections extending
82 down the spinal cord have only been shown in rodents, though sparse
83 projections from the deep cerebellar nuclei to the PPN have been
84 shown in primates (Hazrati and Parent, 1992) and spinal cord
85 connections are also suspected to exist in primates (Lee et al., 2000;
86 Pahapill and Lozano, 2000; Matsumura et al., 2000). Recently, we
87 have used probabilistic diffusion tractography (PDT) to trace
88 connections of the PPN in humans (Muthusamy et al., in press).
89 These results show that PPN connections in humans largely match
90 those in primates, but also include descending cerebellar connec-
91 tions. These differing results illustrate the importance of verifying
92 the existence of PPN connections across different species using the
93 same methodological techniques.

94 In contrast to the PPN, the connections of the STN have been well
95 characterized in both rodents and primates and there is little
96 difference between the species (Hamani et al., 2004). The major
97 connections of the STN are with the globus pallidus (GP) and
98 substantia nigra pars reticula (SNpr). The STN also receives
99 excitatory input from various parts of the cerebral cortex, including
100 the motor cortex, SMA, and the dorsal and ventral PMC (dPMC and
101 vPMC, respectively) (Hamani et al., 2004).

102 The current study investigated the topography of STN and PPN
103 connections. Until now, PPN topography has been explored only in
104 primates and has only been demonstrated for cortical connections in
105 one study (Matsumura et al., 2000). However, PPN topography has
106 not been demonstrated in humans or in other species. Distinct
107 topography has also been demonstrated in the STN, separating STN
108 regions connected to motor, associative, and limbic brain areas
109 (Hamani et al., 2004) but has not previously been studied in humans.

110 We used diffusion tensor imaging (DTI) to test for topographic
111 organization in the cortical and subcortical connections of human
112 STN and PPN. DTI can be used to estimate anatomical connections in
113 the human brain *in vivo*. Probabilistic methods for tractography
114 (Parker et al., 2003; Behrens et al., 2003b) allow for tracking of
115 probable fiber pathways between cortical and subcortical grey matter
116 structures (Behrens et al., 2003a; Johansen-Berg et al., 2005; Sillery
117 et al., 2005; Muthusamy et al., in press). For the purposes of this study,
118 connections refer to the estimated anatomical pathways between brain
119 regions (e.g., a fiber path estimated between the STN and a cortical
120 brain region) while topography refers to the size and spatial
121 distribution of the specific parts of a given grey matter structure that
122 connect to other brain regions (e.g., the anterior–medial part of the
123 STN connects with cortical areas). Note that here we are using the
124 terms “connections” and “topography” in a purely anatomical sense.
125 Although tractography cannot determine the direction or sign of
126 functional projections between regions, it does allow for the
127 estimation of the connections and topography of a given brain
128 region, *in vivo*. Therefore, in order to further anatomically characterize
129 human PPN and STN, we have employed PDT to determine the
130 anatomical connections and topography of cortical and subcortical
131 connections of the PPN and STN in healthy human subjects.

132 Methods

133 Subjects and image acquisition

134 Magnetic resonance data were acquired from eight healthy
135 right-handed adult subjects (4 men, 4 women, age range 21–

34 years) with no history of psychiatric or neurological disease. All
subjects provided written informed consent in accordance with
ethical approval from the Central Office for Research Ethics
Committees. A 1.5-T Siemens Sonata MR scanner with maximum
gradient strength of 40 mT m⁻¹ was used. Diffusion-weighted data
were acquired using echo planar imaging (72×2 mm thick axial
slices, matrix 128×104, field of view 256×208 mm, giving a
voxel size of 2×2×2 mm). The diffusion weighting was
isotropically distributed along 60 directions using a *b* value of
1000 s mm⁻¹. A T1-weighted anatomical image was also acquired
using a 3D flash sequence (repetition time=12 ms, echo
time=5.65 ms, and flip angle=19°, with elliptical sampling of *k*
space, giving a voxel size of 1×1×1 mm in 5 min and 5 s).

Image pre-processing

Tools from the FMRIB Software library (FSL, www.fmrib.ox.ac.uk/fsl; Smith et al., 2004) were used for image processing and
analysis. Diffusion-weighted, T1-weighted structural, and MNI
standard brain template images (Evans et al., 2003) were skull-
stripped using the FSL Brain Extraction Tool. Affine registration was
then performed to derive transformation matrices among the three
spaces (diffusion, structural, and standard space). Lastly, probability
distributions of fiber direction at each voxel were calculated using
previously described methods (Behrens et al., 2003b).

Determining regions strongly interconnected to the PPN or STN with probabilistic tractography

We first wished to define the major anatomical connections of
PPN and STN in the human brain. It is difficult to visualize the
boundaries of PPN and STN on diffusion images, and therefore
for this initial analysis, we identified only single seed voxels that
we could be confident were located within the PPN or STN.
These seeds were selected bilaterally for each subject from
transverse slices in diffusion space. The voxel used as the PPN
seed was located at the level of the superior cerebellar peduncle,
in between the medial lemniscus and the superior cerebellar
decussation (SCD) (Figs. 1 and 4A). The SCD is clearly visible
on the RGB representation of the principle diffusion estimate at
each voxel (Stieltjes et al., 2001) and so this representation was
used to ensure that fibers of the SCD did not overlap with the
PPN seed voxel (Fig. 1). The STN single voxel seed was located
at the level of the superior-most slice showing the red nucleus,
medial to the substantia nigra, in the middle of the cerebellar
peduncle (Fig. 6A). These seed voxel locations were indepen-
dently confirmed to be within the PPN and STN by two licensed
neurologists (KA, TZ).

Using FMRIB’s Diffusion Toolbox (FDT, www.fmrib.ox.ac.uk/fsl), fiber tracking was initiated from the single voxel seeds (5000
streamline samples, step length of 0.5 mm, curvature threshold of
0.2, excluding connections crossing into the contralateral hemi-
sphere). Areas displaying connections with the single voxel seed in
at least half of all subjects were determined to be regions with high
probability of connection to the PPN or STN.

Creating anatomical ROIs of interconnected regions

In further analyses, we wished to characterize the topography of
STN and PPN connections with cortical and subcortical regions we
had defined as being strongly interconnected with STN and PPN.

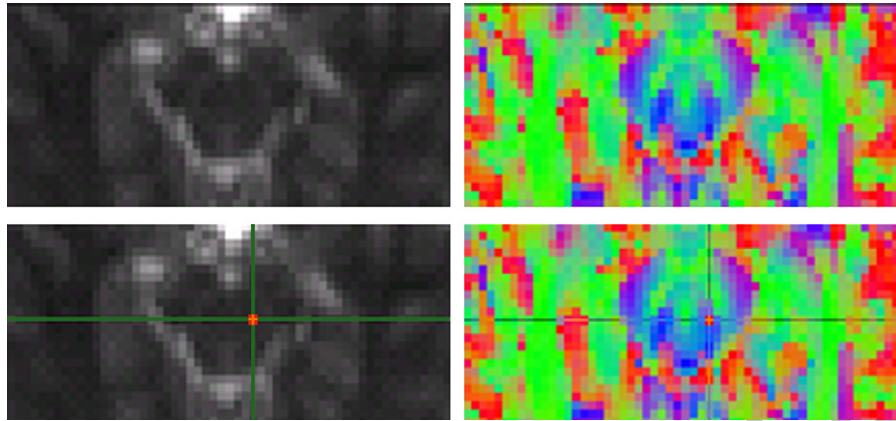


Fig. 1. Localization of PPN seed voxels. A transverse brain slice from one subject is shown as DTI images in diffusion space. In the bottom images, the cross hairs and orange square indicate the location of a PPN seed voxel. The images on the right are the RGB representations of the principle diffusion estimate at each voxel. In the RGB images, the superior cerebellar decussation is clearly visible as a green area in the center of the brainstem. In the bottom right RGB image, the superior cerebellar decussation is delineated by a white outline (Stieltjes et al., 2001). (For interpretation of the references to colour in this figure legend, the reader is referred to the web version of this article.)

191 Masks were therefore drawn of these cortical and subcortical target
 192 regions bilaterally on the T1-weighted structural images for each
 193 subject based on visible anatomical landmarks and with reference
 194 to the *Atlas of Neuroanatomy and Neurophysiology* (Netter et al.,
 195 2002). Somatotopic divisions of the motor cortex were estimated as
 196 percentages of the precentral gyrus based on the motor
 197 homunculus. These divisions, from medial to lateral, are legs and
 198 hips (M1-hind), 7.5%; trunk region (M1-trunk), 17.5%; arm and
 199 forearm (M1-fore-U), 15%; wrist and hand (M1-fore-L), 30%; and
 200 neck and orofacial region, 30% (Fig. 2). The SMA and the dPMC
 201 were located just anterior to the precentral sulcus on the medial and
 202 lateral brain surface, respectively. The border between the SMA
 203 and dPMC was set at the same position, mediolaterally, as the
 204 border between M1-trunk and M1-fore-U. The lateral/inferior
 205 border of the dPMC was at the same position, mediolaterally, as a
 206 transverse plane through the midpoint of M1-fore-L (Fig. 2). The
 207 masks were registered to the diffusion data of the same subject
 208 using FMRIB's Linear Image Registration Tool (FLIRT, [www.
 209 fmrib.ox.ac.uk/fsl](http://www.fmrib.ox.ac.uk/fsl)). Mask size did not significantly differ between
 210 hemispheres or across subjects when normalized to each subject's
 211 brain size (paired *t*-test, $p > 0.05$).

Determination of the topography of STN and PPN connections 212

To investigate the topography of anatomical connections from 213
 each nucleus, we created seed masks, surrounding the PPN and 214
 STN single voxel seeds described above, that aimed to include the 215
 entire nucleus of interest (Figs. 5A and 7A). Both the PPN and 216
 STN masks were 36 voxels (288 mm³) in size. The generous size 217
 of the seed mask allowed sufficient space for topography to be 218
 inferred for the PPN and STN and allowed for clear discernment 219
 between areas that preferentially connect with different brain 220
 regions. Tractography was run from every voxel inside these seed 221
 masks and the coordinates of the voxel within each seed mask with 222
 the highest probability of connection to a given brain region was 223
 determined. The locations of these voxels relative to the mid-point 224
 of the seed mask were calculated and these coordinates were 225
 averaged across all 8 patients (16 voxels). The average voxel 226
 location was graphed in the coronal, transverse, and sagittal planes 227
 along with error bars indicating the 95% confidence interval of the 228
 average location. The areas designated by the error bars indicated 229
 the areas of the PPN and STN with highest probability of 230
 connection to other brain structures. An example of topography 231



Fig. 2. Segmentation of cortical regions. Masks of cortical regions are drawn on the T1-weighted structural image from one subject. Left: the motor cortex (shades of red), SMA (dark blue), and dPMC (light blue) are shown on a transverse slice. From medial to lateral, the motor cortex is subdivided into the hindlimb, trunk, upper forelimb, lower forelimb, and orofacial regions. Right: the motor cortex is also visible on a sagittal slice. (For interpretation of the references to colour in this figure legend, the reader is referred to the web version of this article.)

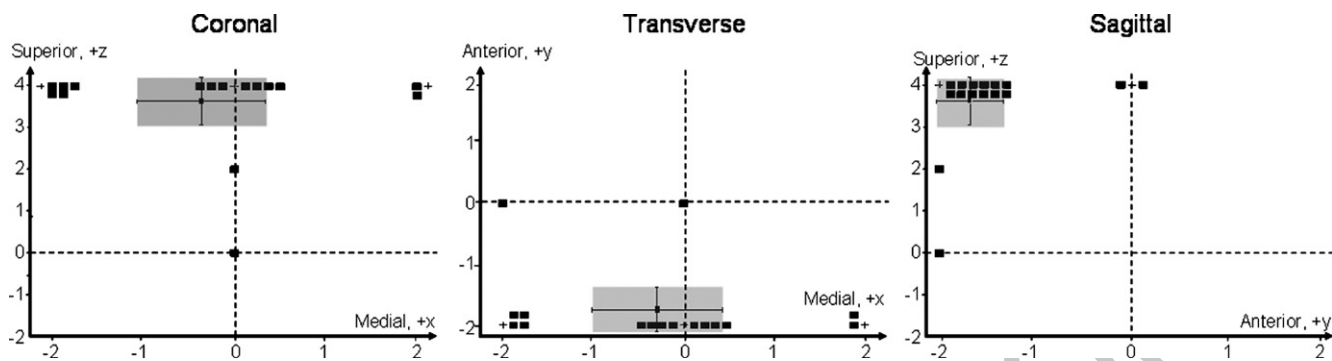


Fig. 3. Example of topography determination. The PPN voxels with highest probability of connection to the thalamus (Fig. 5) are shown in the coronal, transverse, and sagittal planes. The axes show distance in millimeters relative to the midpoint of the PPN seed mask, located at 0 mm on each axis. The two bold dashed lines in each plot intersect at the midpoint of the seed mask. Voxels that have the same coordinates in a given plane are plotted offset from their actual location (indicated by a “+”). The average voxel location is also shown with error bars indicating the 95% confidence interval for each coordinate. This 95% confidence range is shaded grey and indicates the area of the PPN with highest probability of connection to the thalamus.

determination is shown in Fig. 3. In addition to comparing the locations of these PPN and STN regions of connectivity, paired *t*-tests were performed on the *x*, *y*, and *z* coordinates of the PPN and STN voxels to infer existence of topography.

Results

Connections and topography of the PPN

The PPN exhibited connections with the cerebral cortex, basal ganglia, cerebellum, and spinal cord (Table 1, Fig. 4). The cortical regions with high probability of connection to the PPN were the dPMC, SMA, M1-hind, M1-trunk, M1-fore-U, and M1-fore-L (Fig. 4B). Subcortical connections of PPN included the thalamus, GP, and STN (Fig. 4C). In addition, PPN connections were also observed throughout the declive and folium regions of the cerebellum (mid-cerebellum) and extending down the spinal cord (Fig. 4D).

Significant (*p*<0.05) topography in the PPN was present in the coronal (Fig. 5B), transverse (Fig. 5C), and sagittal (Fig. 5D) planes. The anterior and superior portions of the PPN tended to be connected with more anterior and superior brain regions,

respectively. In addition, PPN regions connected to the cortex tended to be located closely together and were generally more laterally located than were PPN regions connected to other brain regions. PPN regions connected to the thalamus, mid-cerebellum, and STN were also located closely together (within the same quadrant of the PPN mask within a given plane). However, the PPN region connected to the GP was distinctly segregated from the regions connecting to other subcortical regions (generally located in the opposite quadrant) (Fig. 5).

Connections and topography of the subthalamic nucleus

The STN also showed high probability of connection to several brain regions (Table 2). In the cortex, connections were found between the STN and the dPMC, SMA, M1-hind, M1-trunk, and M1-fore-U (Fig. 6B). In the basal ganglia, the STN exhibited connections with the thalamus, GP, and SN (Fig. 6C). In addition, STN connections were observed with the PPN, throughout the mid-cerebellum, and extending down the spinal cord (Fig. 6D).

Significant (*p*<0.05) topography was again shown in the STN in the coronal (Fig. 7B), transverse (Fig. 7C), and sagittal (Fig. 7D)

Table 1
PPN connections across all subjects

Brain regions	1L	1R	2L	2R	3L	3R	4L	4R	5L	5R	6L	6R	7L	7R	8L	8R	#	%
Cortex																		
PFC					X	X			X	X							5	31.25
dPMC	X	X	X						X		X		X	X	X		8	50
SMA		X	X	X					X		X		X	X		X	8	50
M1-Hind			X	X	X	X	X		X	X					X		8	50
M1-Trunk		X	X	X	X	X	X	X	X	X	X	X	X	X	X	X	15	93.75
M1-Fore-U	X	X		X	X	X		X	X	X	X	X	X	X	X		13	81.25
M1-Fore-L		X	X	X	X	X	X		X	X	X	X		X	X	X	13	81.25
M1-Orof		X				X					X				X		4	25
Basal ganglia																		
Thalamus	X	X	X	X	X	X	X	X	X	X	X	X	X	X	X	X	16	100
GP	X	X	X	X	X	X	X	X	X	X	X	X	X	X	X	X	13	81.25
STN	X	X	X		X	X	X	X	X	X	X	X	X	X	X		14	87.5
SN		X							X	X						X	4	25
Cerebellum		X	X	X	X	X	X	X	X	X	X	X	X	X	X	X	16	100
Spinal cord		X	X	X	X	X	X	X	X	X	X	X	X	X	X	X	16	100

1L/1R: subject ID left/right PPN; X: regions connected to the indicated PPN as determined from a single PPN seed voxel; #: number of PPNs that are connected to the indicated brain region; %: percentage of PPNs, out of the 16 PPNs examined, that are connected to the indicated brain region.

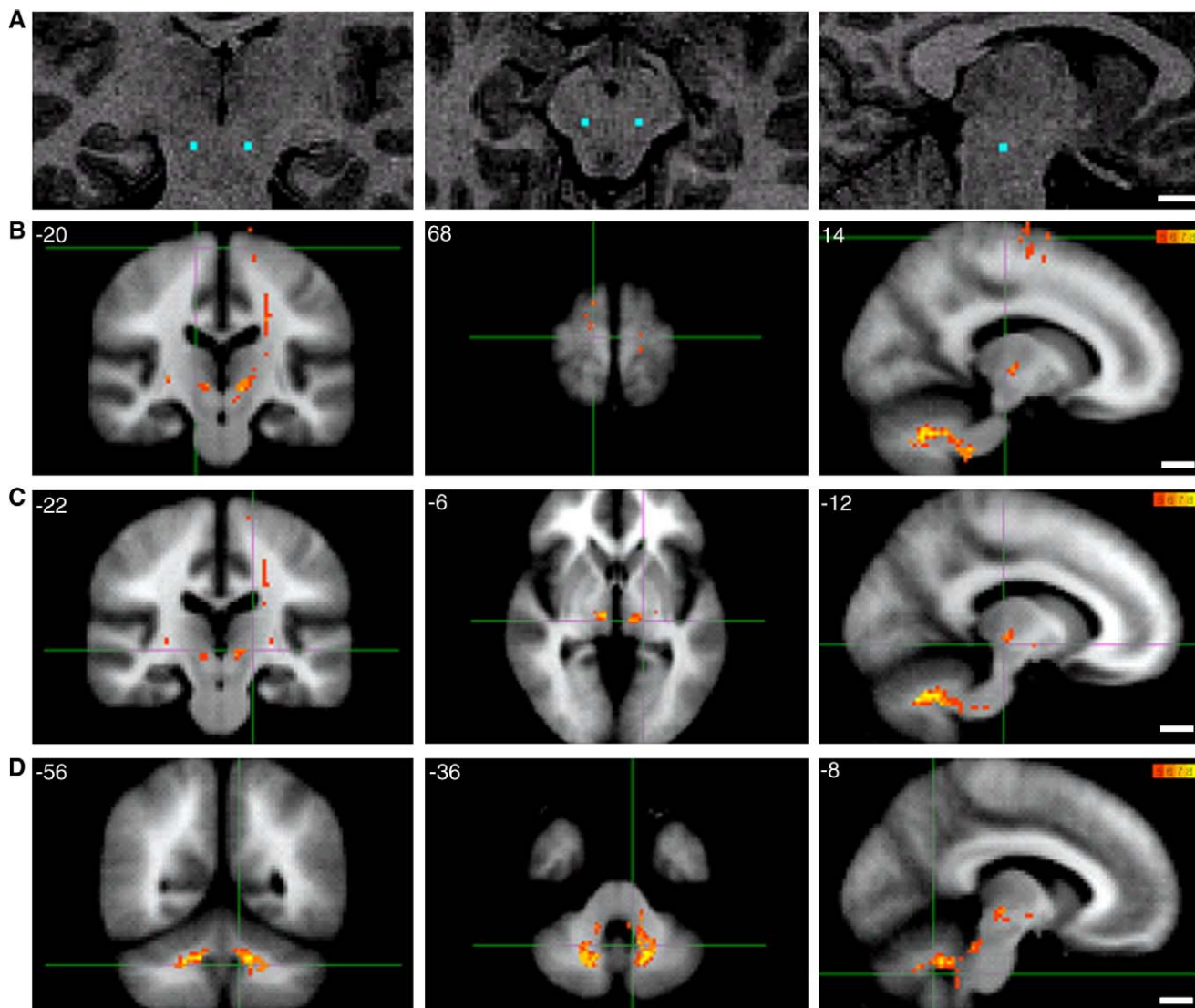



Fig. 4. Regions with highest connectivity to the PPN as determined from a single seed voxel located within the PPN in each hemisphere. (A) Localization of PPN seed voxel ($2 \times 2 \times 2$ mm, selected in diffusion space) is indicated bilaterally by blue squares on a T1-weighted structural image. (B–D) Tracts are thresholded to include projections present in only 4 or more of the 8 subjects. The color of the tract indicates the number of subjects with PPN projections running via a given tract (as shown in the color scale in the upper right corner of each row). Each row shows slices that intersect at the voxel location indicated by the green cross hairs. The MNI coordinate of each slice is also shown in the upper left corner of each brain image. White bars at the lower right hand corner of each row show a 1-cm scale for the figures in that row. (B) Connectivity between the PPN and the motor cortex, SMA, and PMC. (C) Connectivity between the PPN and the pallidum, thalamus, and STN. (D) Connectivity between PPN and the mid-cerebellum and spinal cord. (For interpretation of the references to colour in this figure legend, the reader is referred to the web version of this article.)

271 planes.  shows the location (within a 95% confidence interval
 272 across all subjects) of the STN voxel showing the highest
 273 probability of connection to the indicated brain area. The general
 274 trends in STN topographical organization in the x - and y -directions
 275 matched those in the PPN. STN regions connected to the cortex
 276 were generally more laterally located than STN regions connected
 277 to other brain regions and more anterior portions of the STN tended
 278 to be connected with more anterior brain regions. However, in the
 279 superior–inferior (z -axis) direction, unlike the general trend in the
 280 PPN, the STN regions connected to the cortex tended to be more
 281 superiorly located than regions connecting to other brain areas.
 282 When examining topography trends across planes, STN regions
 283 connected to the dPMC and SMA tended to be segregated from the
 284 STN regions connected to the motor cortex. STN regions

connected to the GP, mid-cerebellum, SN, and PPN were located 285
 closely together (within the same half of the seed mask in a given 286
 plane) in the inferior and medial STN. However, the STN region 287
 connected to the thalamus was distinctly segregated, located 288
 superior and posterior to the STN regions connecting to other 289
 subcortical regions (Fig. 7). 290

Discussion 291

*Human PPN and STN connections largely match connections 292
 previously shown in primates 293*

Table 3 shows a comparison of the connections of the PPN and 294
 STN in humans we determined using PDT with the connections of 295

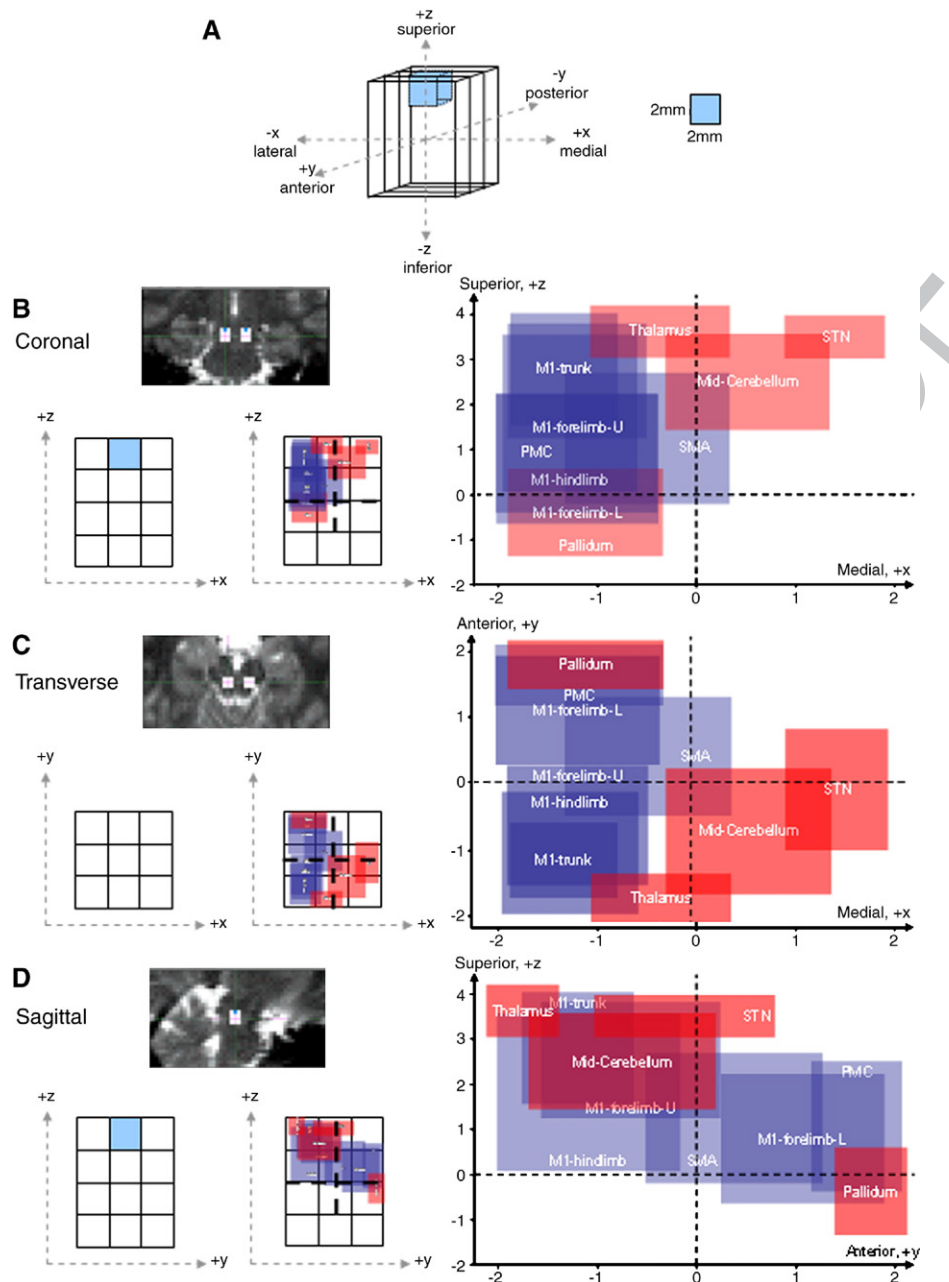


Fig. 5. Topography within the PPN. (A) Schematic of the 36-voxel PPN seed mask. The light blue cube shows the location of the single seed voxel used for the determination of the regions of highest connectivity to the PPN (Fig. 1). (B–D) Seed mask location and topography in the coronal, transverse, and sagittal planes. The left half of each row shows the location of the seed mask in a DTI image in diffusion space (top), a schematic of the seed mask in the given plane (bottom far left), and the topography in that plane (bottom right). Areas of cortical connection are shown in blue and the locations of non-cortical connections are in red. The intersection of the two bold dashed lines in the image showing topography indicates the midpoint of the seed mask. The image on the right of each row zooms in on the areas of highest connectivity as shown in the smaller topography image on the left side of each row. The axes show distance in mm relative to the midpoint of the PPN seed mask, located at 0 mm on each axis. Each red or blue-shaded box is centered at the location of the PPN voxel with the highest probably of connection to the indicated brain region, as determined from the average location across all 8 subjects. The width and height of each box show a 95% confidence interval range, across all 8 subjects, for the location of this PPN voxel (Fig. 3). (For interpretation of the references to colour in this figure legend, the reader is referred to the web version of this article.)

296 the PPN and STN in animals previously determined using tracing
 297 techniques. In humans, both the STN and PPN exhibit connections
 298 with the cortex, basal ganglia, cerebellum, and descending con-
 299 nections via the brainstem to the spinal cord.

300 The major connections of the human PPN determined using
 301 PDT seem to be similar to those seen in lower primates, except that

we did not find strong connections between human PPN and the 302
 substantia nigra. This may represent a key difference between PPN 303
 anatomy in humans and lower primates or may reflect limitations 304
 in our tractography approach. We have also shown a PPN con- 305
 nection in humans that extends down the spinal cord, a connection 306
 that has been demonstrated in rodents but only suspected in 307

t2.1 Table 2

t2.2 STN connections across all subjects

t2.3	Brain regions	1L	1R	2L	2R	3L	3R	4L	4R	5L	5R	6L	6R	7L	7R	8L	8R	#	%
t2.4	Cortex	PFC	X	X		X										X	X	5	31.25
t2.5		dPMC	X	X		X	X	X	X		X		X			X	X	10	62.5
t2.6		SMA	X			X			X	X	X		X			X	X	8	50
t2.7		M1-Hind		X		X		X	X	X			X	X		X	X	9	56.25
t2.8		M1-Trunk	X	X		X	X	X	X	X	X	X		X	X		X	12	75
t2.9		M1-Fore-U	X	X	X	X		X	X	X	X	X	X	X	X		X	14	87.5
t2.10		M1-Fore-L		X	X	X					X					X		6	37.5
t2.11		M1-Orof		X		X	X						X			X		5	31.25
t2.12	Basal ganglia	Thalamus	X	X	X	X	X	X	X	X	X	X	X	X	X	X	X	16	100
t2.13		GP	X	X	X	X	X	X	X	X	X	X	X	X	X	X	X	15	93.75
t2.14		SN	X	X	X	X	X	X	X	X	X	X	X	X	X	X	X	15	93.75
t2.15	PPN		X	X	X	X	X	X	X	X	X	X	X	X	X	X	X	14	87.5
t2.16	Cerebellum			X		X		X	X	X		X		X	X	X	X	12	75
t2.17	Spinal cord		X		X	X	X		X		X	X		X	X	X	X	10	62.5

t2.18 1L/1R: subject ID left/right STN; X: regions connected to the indicated STN as determined from a single STN seed voxel; #: number of STNs that are connected to the indicated brain region; %: percentage of STNs, out of the 16 STNs examined, that are connected to the indicated brain region.

308 primates. In addition to largely matching the PPN connections in
 309 primates, these results also replicate those of our previous study
 310 describing PPN connections in humans using PDT (Muthusamy
 311 et al., in press).

312 The major connections of the human STN are also very similar
 313 to those shown in animal studies except for the presence of mid-
 314 cerebellum and spinal cord connections with the human STN
 315 (Table 3). However, as a strong interconnection between the STN
 316 and PPN has been shown both here and previously (Muthusamy et
 317 al., in press), it is possible that the cerebellar and spinal cord
 318 connections observed with the human STN are actually collaterals
 319 from a strong projection between the human STN and PPN.

320 *Human STN topography matches topography previously shown in*
 321 *animals*

322 The topography of STN connections with motor and associative
 323 brain regions determined in this study exhibits strikingly similar
 324 organization to previous reports of STN topography from rodent
 325 and primate studies (Parent and Hazrati, 1995; Shink et al., 1996;
 326 Joel and Weiner, 1997; Hamani et al., 2004). In all these species,
 327 motor cortical regions (M1, SMA, and dPMC) all connect to the
 328 most superior portion of the STN, while associative regions are
 329 connected to the inferior and medial portions of the STN.

330 It is possible that thalamic fibers running along the superior
 331 border of STN may have been included in the tractography seed
 332 mask, and this may explain why the STN area connected to the
 333 thalamus appears to be segregated from the STN areas connected
 334 to other associative regions. Nevertheless, the use of PDT
 335 demonstrates that the connections and topography of the human
 336 STN largely matches that shown in animal studies. This further
 337 validates the technique and demonstrates its sensitivity.

338 *Demonstration of the existence of PPN topography in humans*

339 We found a clear topography in human PPN connections with
 340 cortical and subcortical areas. Previously, one study in non-human
 341 primates had reported that PPN connections with the orofacial,
 342 forelimb, and hindlimb regions of the primate motor cortex extend,
 343 in that order, from the medial to lateral areas of the nucleus, while
 344 projections to the PMC and SMA are restricted to the middle of the

nucleus (Matsumura et al., 2000). In contrast to the monkey
 345 anatomy, the topography we found in human subjects displayed
 346 little medial to lateral distinction between the different areas of the
 347 human PPN projecting to the cortex. However, we did find a
 348 separation of motor and associative areas of the human PPN, with
 349 connections to motor cortical areas located in the most anterior
 350 portion of the superior PPN.

351 In addition to the cortical PPN topography, we provided the
 352 first demonstration that PPN connections with subcortical brain
 353 regions are topographically organized. The PPN connections with
 354 the thalamus, mid-cerebellum, and STN were primarily located in
 355 the medial, posterior, and superior eighth of the PPN. Interestingly,
 356 the pallidal connections were located in the opposite corner of the
 357 PPN, in the lateral, anterior, and inferior eighth. This is a part of the
 358 PPN seed mask relatively far away from the GP itself, suggesting
 359 that this segregation of pallidal connections is probably not due to
 360 the inclusion of pallidal fibers in the PPN seed mask but is an
 361 accurate depiction of PPN topography.
 362

363 *Functional and therapeutic implications in humans*

364 Strong pallidal connections are observed in both the human
 365 PPN and STN. This supports the idea that the PPN is underactive
 366 in PD patients because it is over inhibited by descending
 367 GABAergic input from the GPi, whereas STN hyperactivity is
 368 due to decreased inhibitory drive from the GPe. Although it has
 369 also been suggested that PPN underactivity in PD could be due to
 370 excessive inhibitory drive from the SN (Lee et al., 2000), the lack
 371 of a strong connection between the PPN and the SN in humans
 372 makes this possibility unlikely.

373 The results showing topography in the STN and PPN have
 374 distinct implications for targeting in functional neurosurgery. For
 375 example, it has been previously suggested that the optimal site for
 376 targeting in the STN should be the area most connected to
 377 sensorimotor brain regions (Romanelli et al., 2004). Our work
 378 shows that this target site should be in the superior portion of the
 379 STN, which has, in fact, been shown to be the optimal target site
 380 (Voges et al., 2002; Lanotte et al., 2002; Hamel et al., 2003;
 381 Godinho et al., 2006; Caire et al., 2006). In addition, as several
 382 studies still dispute that DBS of the STN is more effective than
 383 DBS of GPi for PD (Burchiel et al., 1999; Volkmann, 2004;

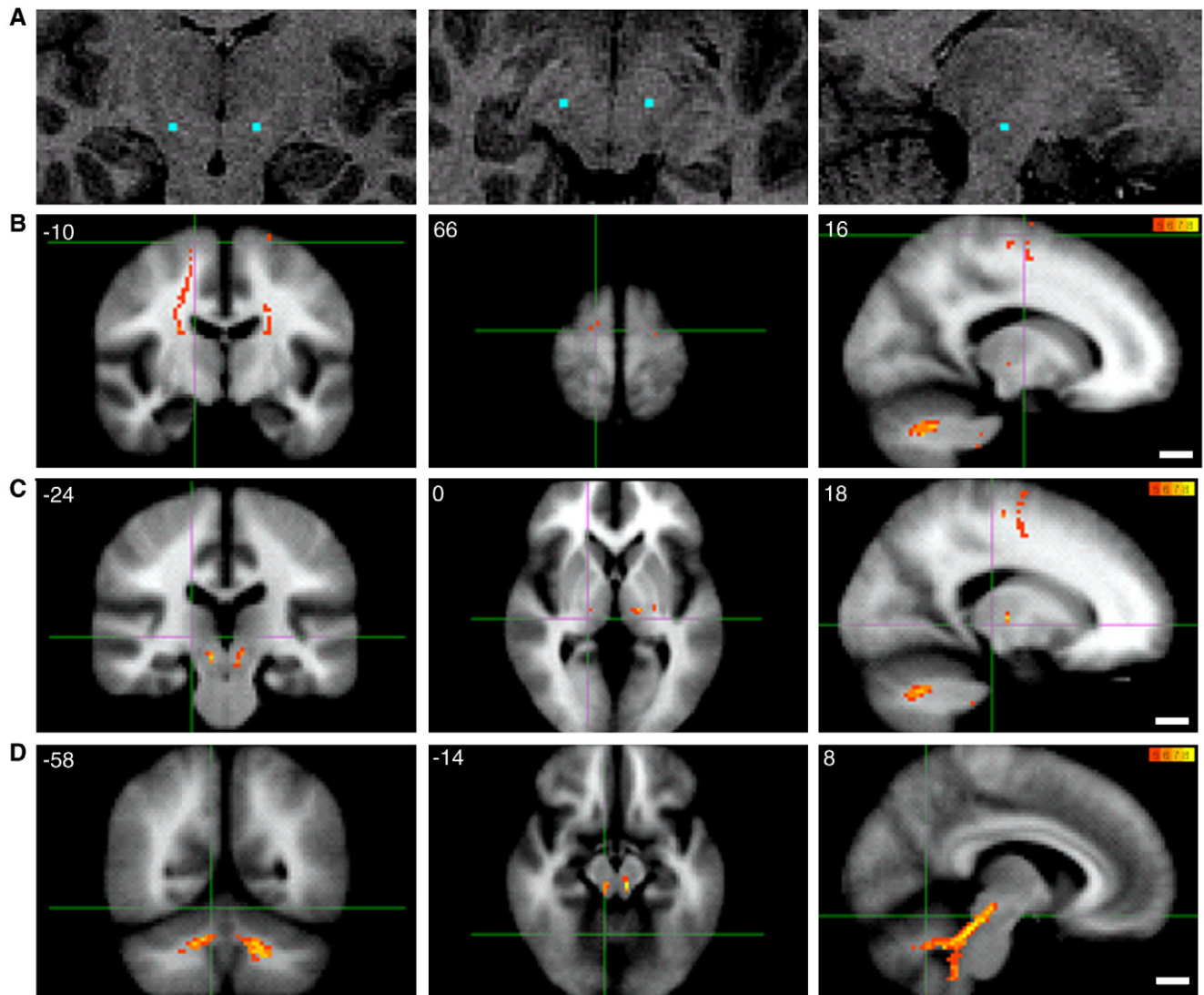


Fig. 6. Regions with highest connectivity to the STN as determined from a single seed voxel located within the STN in each hemisphere. (A) Localization of PPN seed voxel ($2 \times 2 \times 2$ mm, selected in diffusion space) is indicated bilaterally by blue squares on a T1-weighted structural image. (B–D) Tracts are thresholded to include projections present in only 4 or more of the 8 subjects. The color of the tract indicates the number of patients with STN projections running via a given voxel (as shown in the color scale in the upper right corner of each row). Each row shows slices that intersect at the voxel location indicated by the green cross hairs. The MNI coordinate of each slice is also shown in the upper left corner of each figure. White bars at the lower right hand corner of each row show a 1-cm scale for the figures in that row. (B) Connectivity between the STN and the motor cortex, SMA, and PMC. (C) Connectivity between the STN and the pallidum, thalamus, and SN. (D) Connectivity between STN and the PPN, mid-cerebellum, and spinal cord. (For interpretation of the references to colour in this figure legend, the reader is referred to the web version of this article.)

384 Rodriguez-Oroz et al., 2005; Anderson et al., 2005), stimulation of
 385 the portion of the PPN connected with the GP, in addition to STN
 386 stimulation, may be beneficial for PD patients. Though the
 387 directionality of the connection between the GP and PPN cannot
 388 be determined using PDT, it is known that the GPi sends an
 389 inhibitory projection to the PPN in primates. Low frequency
 390 stimulation of the portion of the PPN connected with the GP may
 391 help counter the excessive inhibitory drive from the GPi observed
 392 in PD (Albin et al., 1989; Bergman et al., 1998).

393 Our work shows that sensorimotor brain regions connect with
 394 the lateral half of the PPN and that the GP also connects in the
 395 lateral portion of the PPN, but specifically with the lateral, anterior,
 396 and inferior eighth of the nucleus. Therefore, our PPN topography
 397 results suggest that DBS of the PPN will achieve maximum

therapeutic benefit by specifically targeting this portion of the PPN 398
 for stimulation. This targeting suggestion is especially interesting 399
 when considering preliminary evidence that the beneficial effects 400
 of DBS of the STN and DBS of the PPN in PD patients is additive 401
 (Galati et al., 2006). Perhaps by targeting a portion of the PPN that 402
 does not already connect with the STN, this additive benefit will be 403
 maximized. 404

Methodological considerations 405

There are several methodological issues that should be 406
 considered in interpreting the tractography results presented here. 407
 First, diffusion tractography does not allow us to differentiate 408
 between anterograde and retrograde pathways, inhibitory and 409

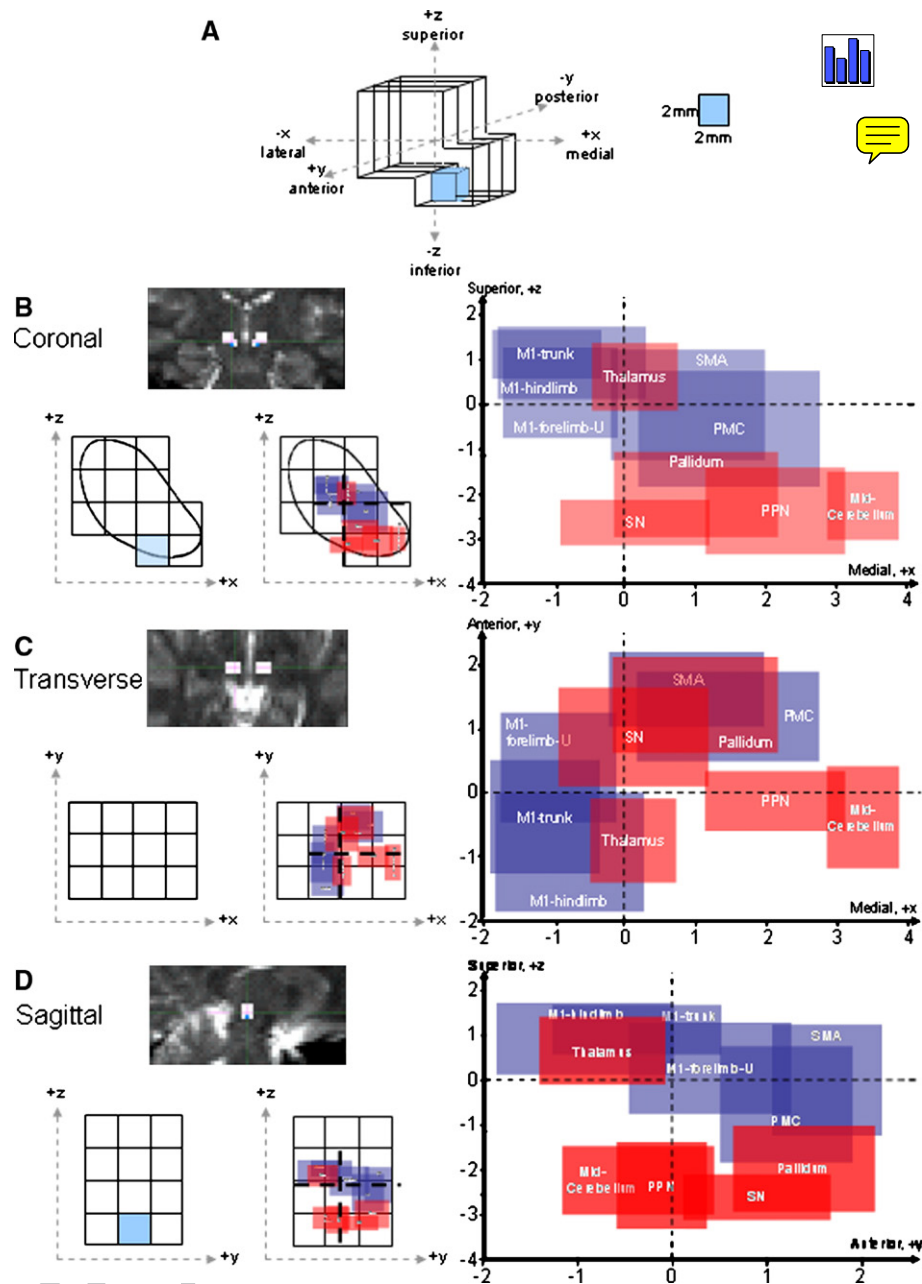


Fig. 7. Topography within the STN. (A) Schematic of the 36-voxel STN seed mask. The light blue cube shows the location of the single seed voxel used for the determination of the regions of highest connectivity to the STN (Fig. 6). (B–D) Seed mask location and topography in the coronal, transverse, and sagittal planes. An outline of the STN is shown overlaid on the seed mask in the coronal view (A). The left half of each row shows the location of the seed mask in a DTI image in diffusion space (top), a schematic of the seed mask in the given plane (bottom far left), and the topography in that plane (bottom right). Locations of cortical connections are shown in blue and non-cortical connections are in red. The intersection of the two bold dashed lines in the image showing topography indicates the midpoint of the seed mask. The image on the right zooms in on the areas of highest connectivity as shown in the smaller topography image on the left side of each row. The axes show distance in mm relative to the midpoint of the STN seed mask, located at 0 mm on each axis. Each red or blue-shaded box is centered at the location of the STN voxel with the highest probability of connection to the indicated brain region, as determined from the average location across all 8 subjects. The width and height of each box show a 95% confidence interval range, across all 8 subjects, for the location of this STN voxel (Fig. 3). (For interpretation of the references to colour in this figure legend, the reader is referred to the web version of this article.)

410 excitatory connections, and direct versus indirect routes. Second,
 411 the tractography is sensitive primarily to large fiber pathways—
 412 smaller pathways, or those through regions of fiber crossing or
 413 complexity may not be detected with the methods used here. This
 414 may have reduced our sensitivity to pathways traveling to lateral
 415 parts of the motor strip. Recently developed models that allow for

modelling of multifiber populations (Hosey et al., 2005; Parker and 416
 Alexander, 2005; Behrens et al., 2007) may improve tracing to 417
 these areas and could be used to interrogate these connections in 418
 the future. Third, the brainstem can suffer from distortions due to 419
 susceptibility gradients; in our data acquired at 1.5 T, however, 420
 such distortions were not substantial and it should be noted that 421

t3.1 Table 3

t3.2 Comparison of human and animal PPN and STN connectivity

t3.3	Connected brain regions	Animal PPN		Human PPN	Animal STN	Human STN
		Rat	Primate			
t3.4						
t3.5	Cortical areas					
t3.6	Motor cortex		X	X	X	X
t3.7	PMC	X	X	X	X	X
t3.8	SMA	X	X	X	X	X
t3.9	Basal ganglia					
t3.10	Thalamus	X	X	X	X	X
t3.11	Pallidum	X	X	X	X	X
t3.12	SN	X	X	X	X	X
t3.13	STN	X	X	X	X	X
t3.14	Cerebellum and brainstem					
t3.15	PPN	X		X		X
t3.16	Mid-cerebellum	X	X	X	X	X
t3.17	Spinal cord	X		X		X

X: regions showing strong connections to the PPN or STN as determined in humans in this DTI study or as determined previously in animals using tracing techniques. Connections in animals characterized as “sparse” or “scant” in the review literature were not included (Lee et al., 2000; Pahapill and Lozano, 2000;

Hamani et al., 2004; Matsumura et al., 2000).

422 previous diffusion studies have successfully traced pathways from
 423 nearby brainstem regions (Stieltjes et al., 2001; Sillery et al., 2005;
 424 Muthusamy et al., in press). Finally, the probability of tracing a
 425 pathway between two points will be influenced by factors other
 426 than the true existence of an anatomical connection—for example,
 427 longer or more tortuous paths are less likely to be traced, although
 428 the topographic distribution of connections is less likely to be
 429 influenced by factors such as distance to the target.

430 Summary and concluding remarks

431 We have provided the first demonstration of topographic
 432 organization of cortical and subcortical connections of STN and
 433 PPN in the human brain. Our data confirm that the STN
 434 topography found in animals is also present in humans. This
 435 provides validation of the accuracy of PDT in determining the
 436 topography of small grey matter structures, such as the STN and
 437 PPN. We have also demonstrated that topography exists in the
 438 human PPN and that there is a distinction between PPN areas
 439 connected to cortical and subcortical structures. Furthermore, the
 440 existence of strong pallidal connections and the absence of strong
 441 nigral connections with the PPN in humans suggests that pallidal
 442 inhibition, rather than inhibitory drive from the SN, may be an
 443 important factor in PPN underactivity in PD. Finally, we use the
 444 PPN topography results to suggest an optimal target site for DBS
 445 of the PPN in PD patients.

446 As aforementioned, it is important to confirm that PDT results
 447 in humans can be reproduced in other species. This is especially
 448 true in the case of the PPN, a structure whose connections differ
 449 greatly across species. Studies examining the connections and
 450 topography of the STN and PPN in primates can be compared
 451 directly to the results of primate anatomical tracing studies. This
 452 could further validate the use of PDT to non-invasively determine
 453 the connections and topography of small grey matter structures as
 454 we have done here for the human PPN and STN.

455 Acknowledgments

456 Funded by the UK MRC (HJB, TZ, JS). We are also grateful for
 457 financial support from the Wellcome Trust (HJB) and the George
 458 C. Marshall Commission (BA).

References

- 459
- Albin, R.L., Young, A.B., Penney, J.B., 1989. The functional anatomy of
 basal ganglia disorders. *Trends Neurosci.* 12, 366–375. 460
- Anderson, V.C., Burchiel, K.J., Hogarth, P., Favre, J., Hammerstad, J.P.,
 2005. Pallidal vs subthalamic nucleus deep brain stimulation in
 Parkinson disease. *Arch. Neurol.* 62, 554–560. 461
- Behrens, T.E., Johansen-Berg, H., Woolrich, M.W., Smith, S.M., Wheeler-
 Kingshott, C.A., Boulby, P.A., Barker, G.J., Sillery, E.L., Sheehan, K.,
 Ciccarelli, O., Thompson, A.J., Brady, J.M., Matthews, P.M., 2003a.
 Non-invasive mapping of connections between human thalamus and
 cortex using diffusion imaging. *Nat. Neurosci.* 6, 750–757. 462
- Behrens, T.E., Woolrich, M.W., Jenkinson, M., Johansen-Berg, H., Nunes,
 R.G., Clare, S., Matthews, P.M., Brady, J.M., Smith, S.M., 2003b.
 Characterization and propagation of uncertainty in diffusion-weighted
 MR imaging. *Magn. Reson. Med.* 50, 1077–1088. 463
- Behrens, T.E., Berg, H.J., Jbabdi, S., Rushworth, M.F., Woolrich, M.W.,
 2007. Probabilistic diffusion tractography with multiple fiber orienta-
 tions: what can we gain? *NeuroImage* 34, 144–155. 464
- Bejjani, B.P., Gervais, D., Arnulf, I., Papadopoulos, S., Demeret, S., Bonnet,
 A.M., Cornu, P., Damier, P., Agid, Y., 2000. Axial parkinsonian
 symptoms can be improved: the role of levodopa and bilateral
 subthalamic stimulation. *J. Neurol. Neurosurg. Psychiatry* 68, 595–600. 465
- Bergman, H., Feingold, A., Nini, A., Raz, A., Slovlin, H., Abeles, M.,
 Vaadia, E., 1998. Physiological aspects of information processing in the
 basal ganglia of normal and parkinsonian primates. *Trends Neurosci.* 21,
 32–38. 466
- Burchiel, K.J., Anderson, V.C., Favre, J., Hammerstad, J.P., 1999.
 Comparison of pallidal and subthalamic nucleus deep brain stimulation
 for advanced Parkinson’s disease: results of a randomized, blinded pilot
 study. *Neurosurgery* 45, 1375–1382. 467
- Caire, F., Derost, P., Coste, J., Bonny, J.M., Durif, F., Frenoux, E., Villeger,
 A., Lemaire, J.J., 2006. Subthalamic deep brain stimulation for severe
 idiopathic Parkinson’s disease Location study of the effective contacts.
Neurochirurgie 52, 15–25. 468
- Evans, A.C., Collins, D.L., Mills, S.R., Brown, E.D., Kelly, R.L., 2003. 3-D
 statistical neuroanatomical models from 305 MRI volumes. *Proc. IEEE*
Nucl. Sci. Symp. Med. Imaging Conf. 1813–1817. 469
- Galati, S., Tropepi, D., Mazzone, P., Stanzione, P., Scarnati, E., Stefani, A.,
 2006. Targeting PPN and STN in severe Parkinsonian patients:
 electrophysiological and clinical findings. *Society for Neuroscience*
 2006 Neuroscience Meeting Planner, Online. 413.8. 470
- Garcia-Rill, E., Skinner, R.D., 1987a. The mesencephalic locomotor region.
 I. Activation of a medullary projection site. *Brain Res.* 411, 1–12. 471
- Garcia-Rill, E., Skinner, R.D., 1987b. The mesencephalic locomotor region.
 II. Projections to reticulospinal neurons. *Brain Res.* 411, 13–20. 472
- 473
- 474
- 475
- 476
- 477
- 478
- 479
- 480
- 481
- 482
- 483
- 484
- 485
- 486
- 487
- 488
- 489
- 490
- 491
- 492
- 493
- 494
- 495
- 496
- 497
- 498
- 499
- 500
- 501
- 502
- 503

- 504 Garcia-Rill, E., Houser, C.R., Skinner, R.D., Smith, W., Woodward, D.J.,
505 1987. Locomotion-inducing sites in the vicinity of the pedunculopontine
506 nucleus. *Brain Res. Bull.* 18, 731–738.
- Q1 507 Godinho, F., Thobois, S., Magnin, M., Guenot, M., Polo, G., Benatru, I.,
508 Xie, J., Salvetti, A., Garcia-Larrea, L., Broussolle, E., Mertens, P., 2006.
509 ~~Subthalamic nucleus stimulation in Parkinson's disease: anatomical and~~
510 ~~electrophysiological localization of active contacts.~~ *J. Neurol.*
511 Hamani, C., Saint-Cyr, J.A., Fraser, J., Kaplitt, M., Lozano, A.M., 2004. The
512 subthalamic nucleus in the context of movement disorders. *Brain* 127,
513 4–20.
- 514 Hamel, W., Fietzek, U., Morsnowski, A., Schrader, B., Herzog, J., Weinert,
515 D., Pfister, G., Muller, D., Volkmann, J., Deuschl, G., Mehdorn, H.M.,
516 2003. Deep brain stimulation of the subthalamic nucleus in Parkinson's
517 disease: evaluation of active electrode contacts. *J. Neurol. Neurosurg.*
518 *Psychiatry* 74, 1036–1046.
- 519 Hazrati, L.N., Parent, A., 1992. Projection from the deep cerebellar nuclei to
520 the pedunculopontine nucleus in the squirrel monkey. *Brain Res.* 585,
521 267–271.
- 522 Hossey, T., Williams, G., Ansoorge, R., 2005. Inference of multiple fiber
523 orientations in high angular resolution diffusion imaging. *Magn. Reson.*
524 *Med.* 54, 1480–1489.
- 525 Jenkinson, N., Nandi, D., Miall, R.C., Stein, J.F., Aziz, T.Z., 2004.
526 Pedunculopontine nucleus stimulation improves akinesia in a Parkin-
527 sonian monkey. *NeuroReport* 15, 2621–2624.
- 528 Joel, D., Weiner, I., 1997. The connections of the primate subthalamic
529 nucleus: indirect pathways and the open-interconnected scheme of basal
530 ganglia-thalamocortical circuitry. *Brain Res. Brain Res. Rev.* 23, 62–78.
- 531 Johansen-Berg, H., Behrens, T.E., Sillery, E., Ciccarelli, O., Thompson,
532 A.J., Smith, S.M., Matthews, P.M., 2005. Functional–anatomical
533 validation and individual variation of diffusion tractography-based
534 segmentation of the human thalamus. *Cereb. Cortex* 15, 31–39.
- 535 Kleiner-Fisman, G., Fisman, D.N., Sime, E., Saint-Cyr, J.A., Lozano, A.M.,
536 Lang, A.E., 2003. Long-term follow up of bilateral deep brain
537 stimulation of the subthalamic nucleus in patients with advanced
538 Parkinson disease. *J. Neurosurg.* 99, 489–495.
- 539 Kojima, J., Yamaji, Y., Matsumura, M., Nambu, A., Inase, M., Tokuno, H.,
540 Takada, M., Imai, H., 1997. Excitotoxic lesions of the pedunculopontine
541 tegmental nucleus produce contralateral hemiparkinsonism in the
542 monkey. *Neurosci. Lett.* 226, 111–114.
- 543 Krack, P., Pollak, P., Limousin, P., Benazzouz, A., Benabid, A.L., 1997.
544 Stimulation of subthalamic nucleus alleviates tremor in Parkinson's
545 disease. *Lancet* 350, 1675.
- 546 Lanotte, M.M., Rizzone, M., Bergamasco, B., Faccani, G., Melcarne, A.,
547 Lopiano, L., 2002. Deep brain stimulation of the subthalamic nucleus:
548 anatomical, neurophysiological, and outcome correlations with the
549 effects of stimulation. *J. Neurol. Neurosurg. Psychiatry* 72, 53–58.
- 550 Lavoie, B., Parent, A., 1994a. Pedunculopontine nucleus in the squirrel
551 monkey: cholinergic and glutamatergic projections to the substantia
552 nigra. *J. Comp. Neurol.* 344, 232–241.
- 553 Lavoie, B., Parent, A., 1994b. Pedunculopontine nucleus in the squirrel
554 monkey: distribution of cholinergic and monoaminergic neurons in the
555 mesopontine tegmentum with evidence for the presence of glutamate in
556 cholinergic neurons. *J. Comp. Neurol.* 344, 190–209.
- 557 Lavoie, B., Parent, A., 1994c. Pedunculopontine nucleus in the squirrel
558 monkey: projections to the basal ganglia as revealed by anterograde
559 tract-tracing methods. *J. Comp. Neurol.* 344, 210–231.
- 560 Lee, M.S., Rinne, J.O., Marsden, C.D., 2000. The pedunculopontine
561 nucleus: its role in the genesis of movement disorders. *Yonsei Med. J.*
562 41, 167–184.
- 563 Limousin, P., Pollak, P., Benazzouz, A., Hoffmann, D., Le Bas, J.F.,
564 Broussolle, E., Perret, J.E., Benabid, A.L., 1995. Effect of parkinsonian
565 signs and symptoms of bilateral subthalamic nucleus stimulation. *Lancet*
566 345, 91–95.
- 567 Limousin, P., Krack, P., Pollak, P., Benazzouz, A., Ardouin, C., Hoffmann,
568 D., Benabid, A.L., 1998. Electrical stimulation of the subthalamic
569 nucleus in advanced Parkinson's disease. *N. Engl. J. Med.* 339,
570 1105–1111.
- Masdeu, J.C., Alampur, U., Cavaliere, R., Tavoulareas, G., 1994. Astasia 571
572 and gait failure with damage of the pontomesencephalic locomotor
573 region. *Ann. Neurol.* 35, 619–621.
- 574 Matsumura, M., Kojima, J., 2001. The role of the pedunculopontine
575 tegmental nucleus in experimental parkinsonism in primates. *Stereotact.*
576 *Funct. Neurosurg.* 77, 108–115.
- 577 Matsumura, M., Nambu, A., Yamaji, Y., Watanabe, K., Imai, H., Inase, M.,
578 Tokuno, H., Takada, M., 2000. Organization of somatic motor inputs
579 from the frontal lobe to the pedunculopontine tegmental nucleus in the
580 macaque monkey. *Neuroscience* 98, 97–110.
- 581 Mazzone, P., Lozano, A., Stanzione, P., Galati, S., Scarnati, E., Peppe, A.,
582 Stefani, A., 2005. Implantation of human pedunculopontine nucleus: a
583 safe and clinically relevant target in Parkinson's disease. *NeuroReport*
584 16, 1877–1881.
- 585 Munro-Davies, L.E., Winter, J., Aziz, T.Z., Stein, J.F., 1999. The role of the
586 pedunculopontine region in basal-ganglia mechanisms of akinesia. *Exp.*
587 *Brain Res.* 129, 511–517.
- 588 Muthusamy, K.A., Aravamuthan, B.R., Kringelbach, M.L., Voets, N.L.,
589 Johansen-Berg, H., Stein, J., Aziz, T., in press. Connectivity of the
590 human pedunculopontine nucleus region (PPN) and diffusion tensor
591 imaging in surgical targeting. *Journal of Neurosurgery.*
- 592 Nandi, D., Aziz, T.Z., Giladi, N., Winter, J., Stein, J.F., 2002. Reversal of
593 akinesia in experimental parkinsonism by GABA antagonist micro-
594 injections in the pedunculopontine nucleus. *Brain* 125, 2418–2430.
- 595 Netter, F.H., Craig, J.A., Perkins, J., Hansen, J.T., Koeppen, B.M., 2002.
596 *Atlas of Neuroanatomy and Neurophysiology. Selections from the*
597 *Netter Collection of Medical Illustrations. Icon Custom Communica-*
598 *tions, Teterboro NJ.*
- 599 Pahapill, P.A., Lozano, A.M., 2000. The pedunculopontine nucleus and
600 Parkinson's disease. *Brain* 123 (Pt 9), 1767–1783.
- 601 Parent, A., Hazrati, L.N., 1995. Functional anatomy of the basal ganglia. II.
602 The place of subthalamic nucleus and external pallidum in basal ganglia
603 circuitry. *Brain Res. Brain Res. Rev.* 20, 128–154.
- 604 Parker, G.J., Alexander, D.C., 2005. Probabilistic anatomical connectivity
605 derived from the microscopic persistent angular structure of cerebral
606 tissue. *Philos. Trans. R. Soc. Lond., B Biol. Sci.* 360, 893–902.
- 607 Parker, G.J., Haroon, H.A., Wheeler-Kingshott, C.A., 2003. A framework
608 for a streamline-based probabilistic index of connectivity (PICO) using a
609 structural interpretation of MRI diffusion measurements. *J. Magn.*
610 *Reson. Imaging* 18, 242–254.
- 611 Plaha, P., Gill, S.S., 2005. Bilateral deep brain stimulation of the pedunclo-
612 pontine nucleus for Parkinson's disease. *NeuroReport* 16, 1883–1887.
- 613 Rodriguez-Oroz, M.C., Obeso, J.A., Lang, A.E., Houeto, J.L., Pollak, P.,
614 Rehncrona, S., Kulisevsky, J., Albanese, A., Volkmann, J., Hariz, M.I.,
615 Quinn, N.P., Speelman, J.D., Guridi, J., Zamarbide, I., Gironell, A.,
616 Molet, J., Pascual-Sedano, B., Pidoux, B., Bonnet, A.M., Agid, Y., Xie,
617 J., Benabid, A.L., Lozano, A.M., Saint-Cyr, J., Romito, L., Contarino,
618 M.F., Scerrati, M., Fraix, V., Van Blercom, N., 2005. Bilateral deep brain
619 stimulation in Parkinson's disease: a multicentre study with 4 years
620 follow-up. *Brain* 128, 2240–2249.
- 621 Romanelli, P., Bronte-Stewart, H., Heit, G., Schaal, D.W., Esposito, V.,
622 2004. The functional organization of the sensorimotor region of the
623 subthalamic nucleus. *Stereotact. Funct. Neurosurg.* 82, 222–229.
- 624 Rye, D.B., Saper, C.B., Lee, H.J., Wainer, B.H., 1987. Pedunculopontine
625 tegmental nucleus of the rat: cytoarchitecture, cytochemistry, and some
626 extrapyramidal connections of the mesopontine tegmentum. *J. Comp.*
627 *Neurol.* 259, 483–528.
- 628 Shink, E., Bevan, M.D., Bolam, J.P., Smith, Y., 1996. The subthalamic nucleus
629 and the external pallidum: two tightly interconnected structures that control
630 the output of the basal ganglia in the monkey. *Neuroscience* 73, 335–357.
- 631 Sillery, E., Bittar, R.G., Robson, M.D., Behrens, T.E., Stein, J., Aziz, T.Z.,
632 Johansen-Berg, H., 2005. Connectivity of the human periventricular–
633 periaqueductal gray region. *J. Neurosurg.* 103, 1030–1034.
- 634 Smith, S.M., Jenkinson, M., Woolrich, M.W., Beckmann, C.F., Behrens,
635 T.E., Johansen-Berg, H., Bannister, P.R., De Luca, M., Drobnjak, I.,
636 Flitney, D.E., Niazy, R.K., Saunders, J., Vickers, J., Zhang, Y., De
637 Stefano, N., Brady, J.M., Matthews, P.M., 2004. Advances in functional

Q2



- 638 and structural MR image analysis and implementation as FSL. 652
639 *Neuroimage* 23 (Suppl. 1), S208–S219. 653
- 640 Spann, B.M., Grofova, I., 1989. Origin of ascending and spinal pathways 654
641 from the nucleus tegmenti pedunculopontinus in the rat. *J. Comp.* 655
642 *Neurol.* 283, 13–27. 656
- 643 Spann, B.M., Grofova, I., 1991. Nigropedunculopontine projection in the 657
644 rat: an anterograde tracing study with phaseolus vulgaris-leucoagglutinin 658
645 (PHA-L). *J. Comp Neurol.* 311, 375–388. 659
- 646 Spann, B.M., Grofova, I., 1992. Cholinergic and non-cholinergic neurons in 660
647 the rat pedunculopontine tegmental nucleus. *Anat. Embryol. (Berl)* 186, 661
648 215–227. 662
- 649 Stieltjes, B., Kaufmann, W.E., van Zijl, P.C., Fredericksen, K., Pearson, 663
650 G.D., Solaiyappan, M., Mori, S., 2001. Diffusion tensor imaging and 664
651 axonal tracking in the human brainstem. *NeuroImage* 14, 723–735. 665
666
- Stolze, H., Klebe, S., Poepping, M., Lorenz, D., Herzog, J., Hamel, W., 652
Schrader, B., Raethjen, J., Wenzelburger, R., Mehdorn, H.M., Deuschl, 653
G., Krack, P., 2001. Effects of bilateral subthalamic nucleus stimulation 654
on parkinsonian gait. *Neurology* 57, 144–146. 655
- Voges, J., Volkmann, J., Allert, N., Lehrke, R., Koulousakis, A., Freund, 656
H.J., Sturm, V., 2002. Bilateral high-frequency stimulation in the 657
subthalamic nucleus for the treatment of Parkinson disease: correlation 658
of therapeutic effect with anatomical electrode position. *J. Neurosurg.* 659
96, 269–279. 660
- Volkmann, J., 2004. Deep brain stimulation for the treatment of Parkinson's 661
disease. *J. Clin. Neurophysiol.* 21, 6–17. 662
- Yokoyama, T., Sugiyama, K., Nishizawa, S., Yokota, N., Ohta, S., Uemura, 663
K., 1999. Subthalamic nucleus stimulation for gait disturbance in 664
Parkinson's disease. *Neurosurgery* 45, 41–47. 665

UNCORRECTED PROOF